

Choroidal Flow Signal in Late-Onset Stargardt Disease and Age-Related Macular Degeneration: An OCT-Angiography Study

Philipp L. Müller,^{1,2} Maximilian Pfau,^{1,3} Philipp T. Möller,^{1,3} Jennifer Nadal,⁴ Matthias Schmid,⁴ Moritz Lindner,^{1,5} Luis de Sisternes,^{6,7} Heidi Stöhr,⁸ Bernhard H. F. Weber,⁸ Christine Neuhaus,⁹ Philipp Herrmann,^{1,2} Steffen Schmitz-Valckenberg,^{1,3} Frank G. Holz,¹⁻³ and Monika Fleckenstein^{1,3}

¹Department of Ophthalmology, University of Bonn, Bonn, Germany

²Center for Rare Diseases, University of Bonn, Bonn, Germany

³GRADE Reading Center, Bonn, Germany

⁴Institute for Medical Biometry, Informatics and Epidemiology, University Hospital Bonn, Bonn, Germany

⁵The Nuffield Laboratory of Ophthalmology, Sleep and Circadian Neuroscience Institute, Nuffield Department of Clinical Neurosciences, University of Oxford, Oxford, United Kingdom

⁶Department of Radiology, Stanford University, Stanford, California, United States

⁷Carl Zeiss Meditec, Inc., Dublin, California, United States

⁸Institute of Human Genetics, University of Regensburg, Regensburg, Germany

⁹Center for Human Genetics Bioscientia, Ingelheim, Germany

Correspondence: Monika Fleckenstein, University of Bonn, Department of Ophthalmology, Ernst-Abbe-Str. 2, Bonn D-53127, Germany; Monika.Fleckenstein@ukbonn.de.

PLM and MP contributed equally to the work presented here and should therefore be regarded as equivalent authors.

Submitted: January 17, 2018

Accepted: July 18, 2018

Citation: Müller PL, Pfau M, Möller PT, et al. Choroidal flow signal in late-onset Stargardt disease and age-related macular degeneration: an OCT-angiography study. *Invest Ophthalmol Vis Sci*. 2018;59:AMD122-AMD131. <https://doi.org/10.1167/iovs.18-23819>

PURPOSE. To investigate the choroidal blood flow in areas within and adjacent to retinal pigment epithelium (RPE) atrophy secondary to late-onset Stargardt disease (STGD1) and age-related macular degeneration (AMD).

METHODS. A total of 43 eyes (23 STGD1 and 20 AMD) of patients with RPE atrophy and 25 eyes of healthy controls without ocular pathology underwent multimodal imaging including optical coherence tomography angiography (OCT-A; PLEX Elite 9000 Swept-Source OCT). Using an exploratory approach, choriocapillaris and deeper choroid OCT-A slabs were evaluated in order to detect differences between STGD1 and AMD. The magnitude of absence-of-flow signal (AFS) was investigated in terms of area-fraction and size-frequency distribution.

RESULTS. Qualitative and quantitative analysis of areas of RPE atrophy revealed more pronounced rarefaction of the choriocapillaris flow signal in STGD1 as compared to AMD (AFS area fraction: $33.15\% \pm 6.86\%$ vs. $31.68\% \pm 8.39\%$; $P = 0.517$), while outside RPE atrophy rarefaction was less pronounced in STGD1 (AFS area fraction: $17.41\% \pm 5.67\%$ vs. $21.59\% \pm 6.90\%$; $P < 0.001$), to the level of nonsignificance compared to controls ($13.27\% \pm 2.99\%$, $P = 0.368$). Given this discrepancy, the ratio of the AFS area fraction within/outside of RPE atrophy could be used to differentiate between STGD1 and AMD with 65.0% sensitivity and 92.3% specificity.

CONCLUSIONS. Using OCT-A, comparison of choroidal flow signal within and outside the area of RPE atrophy revealed distinct differences between STGD1 and AMD, potentially implicating a differential role of the choroid in the pathogenesis of RPE atrophy in these two diseases.

Keywords: optical coherence tomography angiography, ABCA4, retina, AMD, geographic atrophy

Stargardt disease (STGD1) is the most common single gene retinal dystrophy caused by mutations in the ATP-binding cassette subfamily A member 4 (*ABCA4*, Online Mendelian Inheritance in Man #601691) gene.¹⁻⁵ Dysfunction or loss of function of the encoded protein leads to excessive accumulation of lipofuscin in the lysosomal compartment of retinal pigment epithelium (RPE) cells. Lipofuscin is an intracellular fluorophore that is predominantly derived from vitamin A compounds. It is assumed to have toxic effects on RPE cells and to lead to primary RPE atrophy.^{4,5} Due to its variable clinical presentation, STGD1 can be classified by phenotypic manifes-

tation,^{6,7} or by age of onset in early-onset, intermediate-onset, and late-onset STGD1.⁸

In contrast to STGD1, age-related macular degeneration (AMD), the leading cause of blindness in industrial countries, is a complex, multifactorial disease. Chronic inflammatory processes, lipofuscin accumulation in the RPE, complement system dysregulation, and vascular factors have been implicated in the pathogenesis.⁹ In advanced disease, AMD can present with neovascular and/or atrophic complications. Neovascular AMD is characterized by the growth of abnormal blood vessels accompanied by leakage of fluid and blood. Late-stage



nonexudative AMD, similar to STGD1, is characterized by RPE atrophy at the posterior pole.¹⁰ Thus, similarities in clinical manifestation between late-onset STGD1 and late-stage AMD may result in misdiagnosis of patients.¹¹ In view of the growing number of therapeutic trials,^{12–16} STGD1 and AMD should be distinguished as to pathogenesis, and, therefore, therapeutic approaches are different.

As RPE and the choroid represent a coadjutant functional complex, vascular changes are present in both diseases.^{17–20} Histopathologic studies of STGD1 revealed a loss of choriocapillaris (CC) within areas of RPE atrophy and preserved choroid outside of RPE atrophy.^{21–23} In contrast, AMD as a multifactorial disease showed inconsistent histopathologic results as there may be transition zones from intact to absent CC as well as CC breakdown preceding outer retinal degeneration.^{9,24,25} In this context, hypofluorescence in areas of RPE atrophy during late phases of indocyanine green angiography (ICGA), used to visualize choroidal vasculature,^{26,27} was found to be more common in STGD1 compared to AMD.²⁸

The introduction of optical coherence tomography angiography (OCT-A) allows for noninvasive in vivo visualization of blood flow with three-dimensional resolution. Nevertheless, all reports so far describe a loss of CC within areas of RPE atrophy.²⁹ A recent OCT-A study focusing on the CC layer in areas of RPE atrophy found extensive loss of CC and Sattler's layer in STGD1, whereas AMD patients only showed rarefied CC, suggesting a possible explanation for the different occurrence of “dark atrophy” in ICGA late phase in STGD1 as described before.³⁰ Nevertheless, in areas of RPE atrophy, a quantitative measurement as well as an evaluation of deeper choroidal layers is pending. Furthermore, differences for the area outside of RPE atrophy have not yet been evaluated.

Here, we used noninvasive high-resolution swept-source OCT-A to test the hypothesis that there are differences in choroidal blood flow in areas inside and outside of RPE atrophy in STGD1 and AMD. The aim of the study was to comparatively investigate qualitative and quantitative flow signal alterations in these diseases.

METHODS

This prospective study was performed at the Department of Ophthalmology at the University of Bonn. The study was in adherence with the Declaration of Helsinki. Institutional Review Board approval (Ethikkommission, Medizinischen Fakultät, Rheinische Friedrich-Wilhelms-Universität Bonn, ethics approval ID 089/08 and 027/08), and informed consent from all subjects was obtained.

Patient Characterization

Patients with RPE atrophy areas $\geq 0.05 \text{ mm}^2$ secondary to STGD1 or AMD were included. RPE atrophy was defined as clearly demarcated definitely decreased fundus autofluorescence (FAF) under short-wavelength excitation light (488 nm) in combination with hypertransmission in optical coherence tomography (OCT).^{31,32} Insufficient pupil dilation, additional retinal pathology, previous retinal treatment, or other ocular comorbidities substantially affecting visual function or image quality (e.g., significant media opacity, amblyopia or optic nerve disease) led to exclusion from the study. The diagnosis of AMD was based on soft drusen and other retinal alterations consistent with the disease,⁹ while the diagnosis of STGD1 was based on (1) a compatible phenotype (yellow-white flecks that correlated with hyperautofluorescent flecks on FAF imaging) and (2) the presence of at least one mutated *ABCA4* allele as

well as the absence of mutations in peripherin-2 (*PRPH2*). To avoid potential confounding, patients exhibiting “diffuse-trickling geographic atrophy” were not included, as choroidal insufficiency has been previously implicated in the pathogenesis.^{33–37}

Genetic testing was conducted at the Institute of Human Genetics, University of Regensburg ($n = 7$), and at the Center for Human Genetics Bioscientia, Ingelheim ($n = 6$). Analysis of all coding exons of the *ABCA4* and *PRPH2* genes was done by either direct chain-terminating dideoxynucleotide Sanger sequencing, a custom-designed GeneChip CustomSeq Resequencing Array (RetChip; Affymetrix, Santa Clara, CA, USA), or next-generation sequencing (Regensburg, $n = 5$; Bioscientia, $n = 6$). Two patients (#1 and #3) were screened for known mutations/polymorphisms using the Asper Ophthalmics ABCR400 microarray followed by Sanger sequencing to confirm selected variants.³⁸ Only STGD1 patients with a minimum age of onset (first reported subjective symptoms) of 45 years were included as defined previously.^{38,39} Healthy subjects without retinal pathology served as controls.

Image Acquisition

All subjects underwent a complete ophthalmologic examination including best-corrected visual acuity (BCVA) testing using Early Treatment Diabetic Retinopathy Study (ETDRS) charts,⁴⁰ slit-lamp examination, and funduscopy, as well as a standardized imaging protocol after instillation of 0.5% tropicamide and 2.5% phenylephrine to a pupil diameter of at least 7-mm diameter.

The imaging protocol consisted of fundus photography (Visucam; Carl Zeiss Meditec, Jena, Germany), FAF imaging (488 nm; $30^\circ \times 30^\circ$ square; 1536×1536 pixels) using a confocal scanning laser ophthalmoscope (cSLO; Spectralis HRA; Heidelberg Engineering, Heidelberg, Germany), spectral-domain OCT ($25^\circ \times 30^\circ$; 121 scans with up to 100 images averaged; Spectralis HRA-OCT; Heidelberg Engineering), and OCT-A (PLEX Elite 9000 Swept-Source OCT; Carl Zeiss Meditec, Inc., Dublin, CA, USA). The OCT-A images were acquired using a macula scan pattern of 6×6 -mm field of view, formed by 500 horizontal A-lines at 500 vertical locations with two repeated scans in each fixed location (a total of 500,000 A-lines acquired per OCT-A cube). Each A-line was acquired over a depth of 3 mm and contained 1536 pixels.

Image Processing and Analysis

Areas of RPE atrophy (Area2) and optic nerve head were measured based on FAF images using a semiautomated processing software (RegionFinder, version 2.6.2.0; Heidelberg Engineering), previously validated for retinal degenerations.^{41–43} In the presence of questionably decreased FAF, the structural swept-source OCT data were also taken into account. Specifically, we evaluated the structural data for presence/absence of RPE atrophy and hypertransmission of signal into choroid. The area outside of RPE atrophy excluding the optic nerve head was defined as Area1.

Three-dimensional OCT-A data were processed by a general sliding slab method in order to remove decorrelation tail artifacts within the volume (Fig. 1) (Bagherinia H, et al. *IOVS* 2017;58:ARVO E-Abstract 643). OCT-A en face images were then generated from the artifact-corrected volume using a maximum-intensity projection of the following defined slabs, using the segmentation surfaces: inner limiting membrane segmentation to the RPE segmentation (“whole retina slab”); +10 to +40 μm interval beneath the RPE-Fit segmentation (with positive sign indicating increase in depth), presumably representing predominantly CC blood flow (“CC-slab”); and

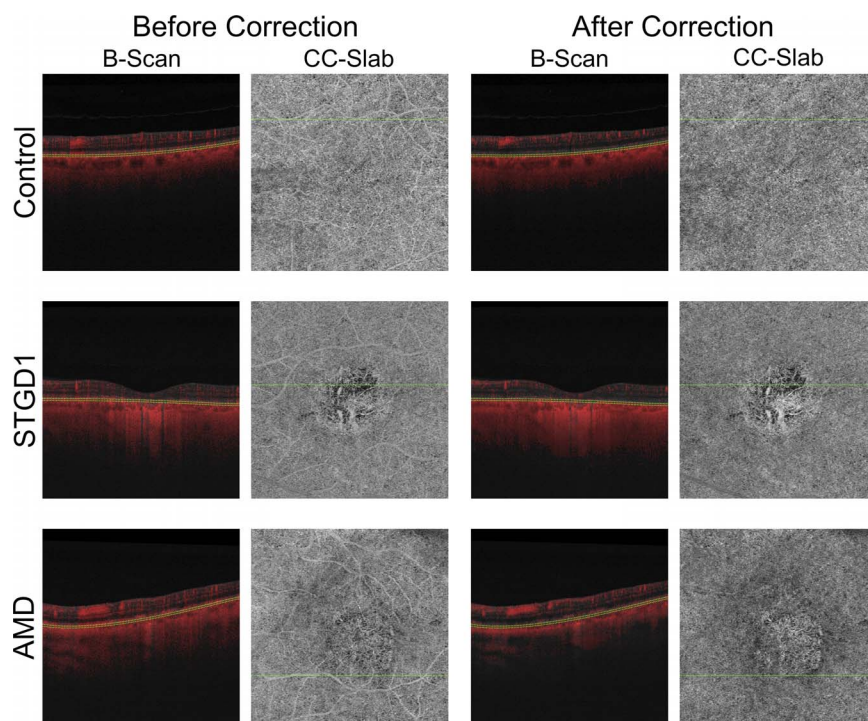


FIGURE 1. Removing decorrelation tail artifacts in optical coherence tomography angiography images. The optical coherence tomography angiography (OCT-A) en face images of the choriocapillaris slab (RPE-Fit segmentation [$+10\ \mu\text{m}$, $+40\ \mu\text{m}$], maximum-intensity projection) and the corresponding B-scans (grayscale depicting the structural OCT data and red depicting OCT-A flow signal) are shown. The two left columns depict the OCT-A data prior to artifact removal. The two right columns were generated using a general sliding slab method to remove decorrelation tail artifacts (Bagherinia H, et al. *IOVS* 2017;58:ARVO E-Abstract 643). Consequently, the artifacts due to the presence of superficial retinal vessels disappear in the corrected en face image. The corresponding B-scan reveals the marked reduction of decorrelation tail artifacts. The dotted green lines in the B-scans indicate the limits of the slab definition shown in the corresponding en face images. The dotted green line in the en face images indicates the location of the corresponding B-scans shown within the en face field of view.

$+64\ \mu\text{m}$, $+115\ \mu\text{m}$ interval beneath the RPE-Fit segmentation, presumably representing deeper choroidal blood flow (“CH-slab”). To improve signal-to-noise ratio in the CC-slab, image processing was applied (Supplementary Material): (1) The imaging data was downsampled to 512×512 pixels. Thus, each pixel represented the average of four pixels leading to noise reduction since noise tended to follow a random pattern, while flow signal or absence-of-flow signal (AFS) was spatially correlated. (2) Taking information from the structural OCT data, a compensation of signal attenuation was achieved and shadowing by flecks or drusen could be minimized in analogy to a previously described method.⁴⁴

Further, we reanalyzed all data using a second more conservative approach by excluding all areas of flecks and/or drusen, as presented in Supplementary Material (see Ref. 45).

FAF images with the respective grading were subsequently registered to the OCT-A data based on vessel bifurcations using ImageJ 1.51j-based FIJI (National Institutes of Health, Bethesda, MD, USA). Besides exemption of potentially side-gated papillary areas and peripapillary atrophy, OCT-A images of CC and CH layer were evaluated to exclude images with artifacts (e.g., due to unstable fixation) as well as shadows (e.g., by floaters) from further analysis.

Areas with AFS of at least 1 pixel (originally 4 pixels) were identified by automatic local thresholding with the Phansalkar method⁴⁶ using a radius of 13 pixels (Fig. 2; equivalent to $152\ \mu\text{m}$ for the image size of 512×512 pixels [$6 \times 6\ \text{mm}$]) as previously proposed by Spaide.⁴⁷ The AFS area fraction for the region inside and the region outside the RPE atrophy in CH and CC OCT-A slabs was then calculated by dividing the number of pixels with AFS by the total number of included pixels of the

respective region. Using the “Analyze Particles” command, the number and size of AFS areas were further evaluated for CC outside the RPE atrophy. As previously described,⁴⁷ the results were logarithmically binned and fitted with a linear trendline that followed the form $\log_{10}(n) = m \cdot \log_{10}(\text{size}) + b$. Hereby, the y -intercept (b) and slope (m) are representative of the number and the proportion of large to small AFS areas, respectively.

Statistical Analysis

Statistical analysis was performed using the software environment R (version 3.2.3; R Foundation for Statistical Computing, Vienna, Austria).⁴⁸ Continuous variables were described by using the mean \pm standard deviation and categorical variables were analyzed using frequency tables. A P value < 0.05 was considered significant.

Mixed-effects models were used to account for the hierarchical nature of the data (eye nested in patient).⁴⁹ To assess the significance of the multilevel variable diagnosis (i.e., control, AMD, STGD1) a post hoc test (Tukey) was used. Since the STGD1 patients and controls were slightly younger than the AMD patients (1-way ANOVA with post hoc Tukey honestly significantly different [HSD] test, $P < 0.05$), the analyses included age as explanatory variable. The AFS area fraction in regions of nonatrophic retina was compared among normal eyes and eyes with AMD and STGD1 with adjustment for age and lesion size. Similarly, the distribution of AFS areas in terms of number and size was compared among normal eyes, eyes with AMD and STGD1 based on the y -intercept (b) and slope (m) fitted to the logarithmically binned data. Further, the AFS area fraction within atrophy was compared between eyes with

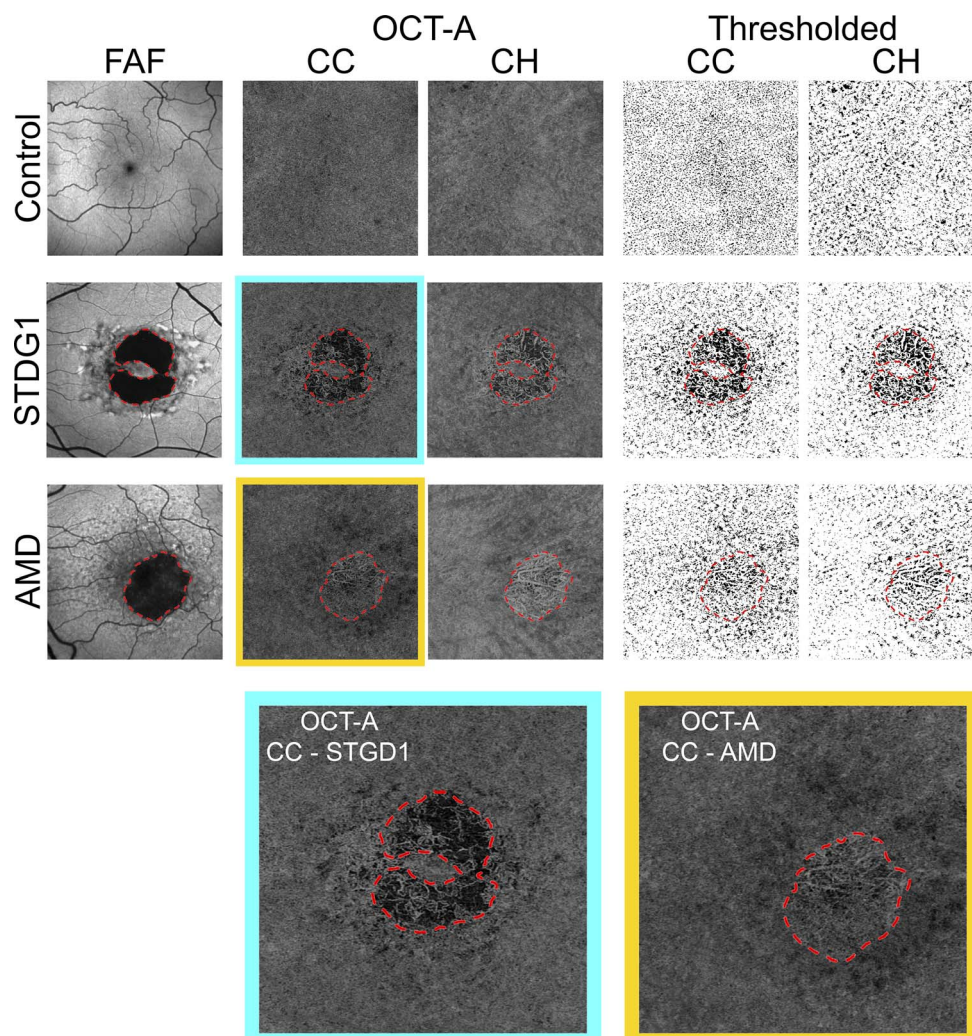


FIGURE 2. Autofluorescence and optical coherence tomography angiography images of exemplary eyes. The fundus autofluorescence (FAF) image of the control reveals relatively uniform signal across the fundus with central shadowing due to macular pigment. In STGD1, pisciform flecks can be observed in STGD1 surrounding the area of the retinal pigment epithelium (RPE) atrophy (delineated by a *red dashed line*), whereas soft drusen and reticular drusen are visible in AMD. The optical coherence tomography angiography (OCT-A) en face image of an exemplary control reveals the dense flow signal texture of the choriocapillaris (CC) slab. The deeper choroid layer (CH) slab is relatively concealed due to preserved retinal pigment epithelium and CC decorrelation tails. Therefore, the CH was evaluated only inside the RPE atrophy in this study. Here, STGD1 revealed more pronounced flow signal alterations in both OCT-A layers up to total loss of the dense flow signal texture with uncovered large-calibered vessels (putative Haller's layer), whereas AMD shows a milder rarefaction of the dense flow signal texture with visibility of mid-calibered vessels (putative Sattler's layer), best visible in *highlighted* images. Outside of the RPE atrophy, both diseases qualitatively show multiple spots with reduced flow signal that are most pronounced in proximity to foci of RPE atrophy. Of note, these changes are more obvious in AMD. The thresholded images were obtained using the Phansalkar method (radius of 13 pixels [corresponding to 152 μ m]) to identify areas with absence-of-flow signal.^{46,47}

AMD and STGD1 as well as the ratio (within-to-outside of RPE atrophy) of the AFS area fraction. Last, receiver operating characteristic (ROC) curves were plotted to evaluate the area under the curve (AUC), diagnostic sensitivity, and specificity for the AFS area fraction within atrophy, outside of atrophy, and for the within-to-outside of atrophy ratio of the AFS area fraction.

RESULTS

Twenty-three eyes of 13 patients with RPE atrophy secondary to STGD1 (age range, 49.9–86.1 years; [mean \pm SD], 66.4 \pm 10.03 years), 20 eyes of 20 patients with RPE atrophy secondary to AMD (age range, 67.7–87.5 years; [mean \pm SD], 78.2 \pm 5.54 years), and 25 eyes of 25 controls (age range, 25.9–84.5 years; [mean \pm SD], 63.5 \pm 16.12 years) were

included. For further characteristics see Table 1. At least two pathogenic or likely pathogenic *ABCA4* mutations were identified in three STGD1 patients (23%), one pathogenic or likely pathogenic *ABCA4* mutation in combination with a variant of unknown significance was found in seven STGD1 patients (54%), and two variants of unknown significance were detected in one STGD1 patient (8%) whereas only one likely pathogenic *ABCA4* mutation was found in two STGD1 patients (15%) (Supplementary Table S1). The frequent c.5603A>T (p.Asn1868Ile) variant recently shown to be associated with STGD1 development, in particular with the late-onset phenotype,^{50,51} was identified in six STGD1 patients. Eleven STGD1 eyes and eight AMD eyes revealed foveal involvement of the RPE atrophy. Correspondingly, visual acuity (LogMAR) was 0.76 \pm 0.70 in STGD1 and 0.51 \pm 0.45 in AMD.

TABLE 1. Demographic and Functional Data of Included Subjects

Subgroup	Controls	STGD1	AMD
Number of patients (female)	25 (7)	13 (8)	20 (12)
Age, y, mean \pm SD	63.48 \pm 16.12	66.36 \pm 10.03	78.18 \pm 5.54
Number of eyes	25	23	20
BCVA in logMAR, mean \pm SD	0.00 \pm 0.00	0.76 \pm 0.70	0.51 \pm 0.45
RPE atrophy in mm ² , mean \pm SD	N/A	10.79 \pm 7.02	6.57 \pm 5.91

NA, not applicable.

Absence-of-Flow Signal Outside of RPE Atrophy

Qualitatively, OCT-A images of controls revealed a dense texture of the CC flow signal with a fine granular appearance and evenly distributed small AFS spots (Fig. 2). Outside the atrophic area, CC flow signal alterations were found in both diseases and appeared to be less pronounced in STGD1 than in AMD. Hereby, AFS spots were more prevalent in proximity to foci of RPE atrophy. These distinct rarefactions of the CC flow signal with prominent AFS spots were associated with the individual presence of flecks or drusen in multimodal imaging, respectively (Fig. 2; Table 2).

Quantitatively, a mixed-effects model revealed that the area outside of RPE atrophy and age as well as the diagnosis had a significant effect on the AFS area fraction (Fig. 3; Table 3). Subsequently, a significant difference was found between STGD1 and AMD as well as controls and AMD (Fig. 3; Table 3). However, the previously described qualitative CC flow signal alterations in STGD1 did not result in a significantly different AFS area fraction compared to controls (post hoc test; STGD1 versus controls: $-2.20\% \pm -1.63\%$, $P = 0.368$; Fig. 3; Table 3).

Individual Flow Texture Outside of RPE Atrophy

To fully consider the individual CC flow signal texture in areas outside of the RPE atrophy, the number and size of AFS spots were analyzed. In all patients and subjects, the graph displaying the size versus number of these AFS spots was highly skewed, with a high number of miniscule AFS spots and few larger AFS spots suggesting that there is a power law relationship between the AFS size and number (Fig. 4; Table 4).

TABLE 2. Results of the Image Analysis (CC-Slab)

Subgroup	Controls, Mean \pm SD	STGD1, Mean \pm SD	AMD, Mean \pm SD
Number of eyes	25	23	20
AFS area fraction outside of RPE atrophy, %	13.27 \pm 2.99	17.41 \pm 5.67	21.59 \pm 6.90
γ -intercept (b) of the AFS log-log size-frequency distribution, log ₁₀ (n)	8.09 \pm 0.44	7.08 \pm 0.65	6.90 \pm 0.63
Slope (m) of the AFS log-log size-frequency distribution, log ₁₀ (n)/log ₁₀ (μ m ²)	-2.10 \pm 0.16	-1.83 \pm 0.19	-1.74 \pm 0.18
AFS area fraction inside of RPE atrophy, %	N/A	33.15 \pm 6.86	31.68 \pm 8.39
AFS area fraction ratio, inside to outside	N/A	2.05 \pm 0.70	1.52 \pm 0.33

NA, not applicable.

In accordance, the corresponding log-log graphs of all patients and controls showed a linear relationship (R^2 of [mean \pm SD] 0.89 ± 0.02 for STGD1, 0.88 ± 0.02 for AMD, and 0.89 ± 0.01 for controls).

The γ -intercept (b) of the linear regression, which reflects the number of AFS spots $\leq 100 \mu\text{m}^2$, was dependent on the diagnosis and area outside of RPE atrophy, while age had no distinct influence (Table 4). In the post hoc comparison, AMD revealed significant lower γ -intercept compared to controls as well as STGD1 (Fig. 4; Table 4). The difference between STGD1 and controls was not significant ($-0.22 \log_{10}(n) \pm 0.17 \log_{10}(n)$, $P = 0.380$).

The slope (m), which reflects the ratio of miniscule to larger AFS spots, was dependent on the diagnosis and area outside RPE atrophy, while age exhibited no significant effect (Table 4). The slope was significantly less negative in AMD compared to controls and STGD1, indicating the presence of more large AFS spots (Fig. 4; Table 4). The difference between STGD1 and controls was again not significant (post hoc test; $0.08 \log_{10}(n)/\log_{10}(\mu\text{m}^2) \pm 0.06 \log_{10}(n)/\log_{10}(\mu\text{m}^2)$, $P = 0.401$).

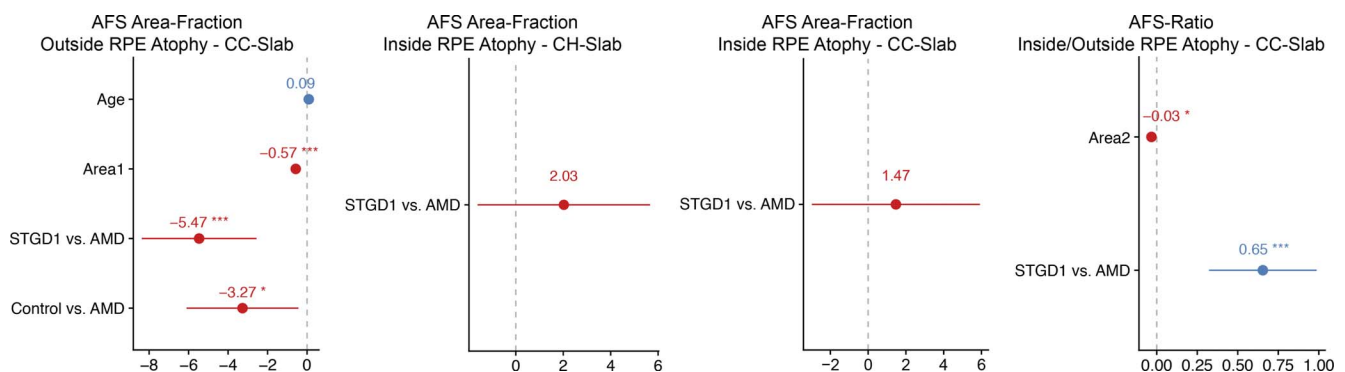


FIGURE 3. Results of the mixed-effects model analysis: the fixed effects and 95% confidence intervals for the mixed-effects models that fully accounted for the hierarchical nature of the data (eye nested in patient). Quantitative evaluation of absence-of-flow signal (AFS) showed significant differences of STGD1 and AMD eyes outside RPE atrophy (Area1). Despite nonsignificant differences inside RPE atrophy (Area2) for choriocapillaris (CC) slab and deeper choroid layer (CH) slab, AFS ratio (inside-to-outside of RPE atrophy) was highly significantly different. The P values were obtained using Wald's test (significance codes: *** $P < 0.001$; ** $P < 0.01$; * $P < 0.05$).

TABLE 3. Results of the Mixed-Effects Models (Estimate of Effect) for Absence-of-Flow Signal (AFS) Analysis

Variable	Estimate	SE*	P Value
AFS area fraction, outside RPE atrophy—CC-slab			
Age, %/y	0.087	0.044	0.049
Area1, %/mm ²	−0.574	0.103	<0.001
Diagnosis			
STGD1 vs. AMD, %	−5.467	1.482	<0.001
Control vs. AMD, %	−3.269	1.446	0.024
AFS area fraction, inside RPE atrophy—CH-slab			
Diagnosis			
STGD1 vs. AMD, %	2.03	1.86	0.275
AFS area fraction, inside RPE atrophy—CC-slab			
Diagnosis			
STGD1 vs. AMD, %	1.471	2.270	0.517
AFS-ratio, inside/outside RPE atrophy—CC-slab			
Area2, %/mm ²	−0.032	0.013	0.011
Diagnosis			
STGD1 vs. AMD, %	0.655	0.169	<0.001

* Standard error.

Absence-of-Flow Signal Within RPE Atrophy

Within the area of RPE atrophy secondary to STGD1 and AMD, the flow signal was qualitatively rarefied or even totally absent, both in the CC-slab and the CH-slab. Qualitatively, the flow signal rarefaction appeared to be more pronounced in STGD1 compared to AMD (Fig. 2). Yet, in quantitative analysis, these higher absolute AFS area fractions (Table 2) did not meet significance levels for the CC-slab as well as the CH-slab (Fig. 3; Table 3).

Ratio of Absence-of-Flow Signal Area Fraction

The opposing properties of AFS in STGD1 and AMD concerning the CC-slab within and outside the area of RPE atrophy suggested that the ratio of the AFS area fractions could provide better diagnostic accuracy than the AFS area fractions themselves (Table 2). Hereby, STGD1 patients exhibited a markedly higher AFS ratio. Of note, the lesion size had also an influence on this specific ratio in our cohort (Table 3).

Diagnostic Accuracy

Finally, ROC curves concerning the diagnostic accuracy of STGD1 and AMD were calculated for the area fraction of AFS outside the RPE atrophy and inside the RPE atrophy as well as for the AFS ratio. For the area fraction of AFS outside the RPE atrophy (AUC of 0.65) and area fraction of AFS inside RPE atrophy (AUC of 0.635), the diagnostic accuracy was similar. The highest differences between STGD1 and AMD could be found when the AFS ratio was considered (AUC, 0.804; Fig. 5). Hence, both disease entities could be separated with 65.0% sensitivity and 92.3% specificity, using a threshold of 0.73 for the AFS ratio.

In order to exclude “shadow artifacts” as potential confounder, we used a further conservative approach by exclusion of all areas of flecks and drusen for analysis. Methods and results of this approach are presented in Supplementary Material. Briefly, similar overall results were obtained.

DISCUSSION

This OCT-A study aimed at quantitative comparison between the choroidal flow signal in RPE atrophy secondary to late-

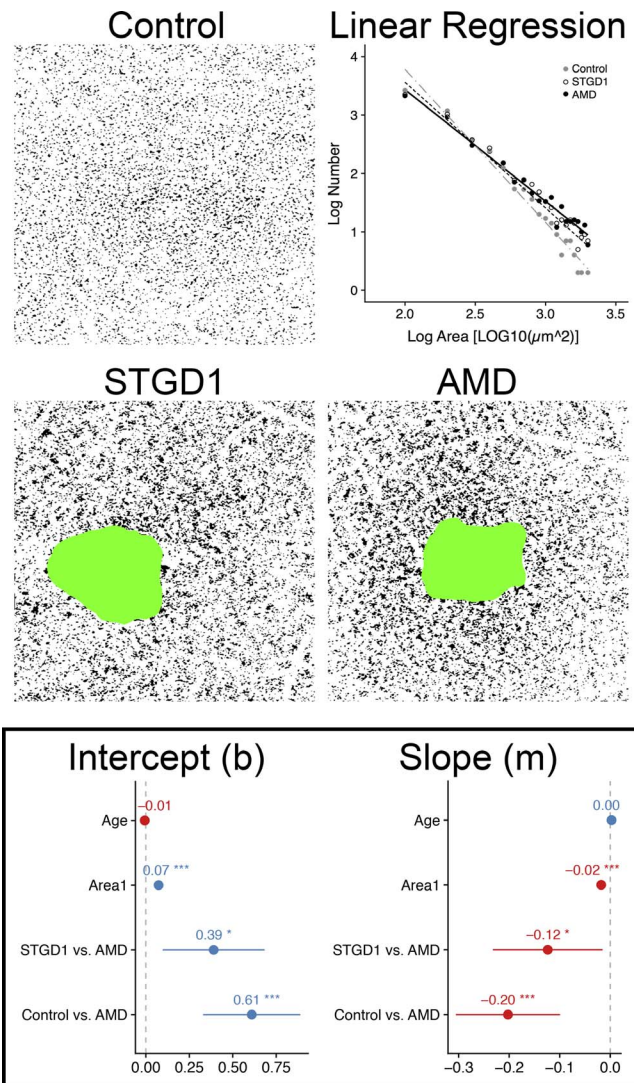


FIGURE 4. Analysis of the vascular texture. The exemplary images were obtained through adaptive local thresholding (Phansalkar method, radius of 13 pixels [corresponding to 152 μm]) to identify areas with absence-of-flow signal (AFS).^{46,47} The area of RPE atrophy (highlighted in green) was excluded from the analysis. The dot plot shows the log-log size-frequency distribution of the areas of AFS for the three exemplary images and the linear regression lines.⁴⁷ Please note, the exemplary AMD eye shows the flattest linear regression indicating a relatively higher proportion of larger areas with AFS compared to the STGD1 eye and control eye. The lower figure parts show the fixed effects and 95% confidence intervals of the mixed-effects models describing the y-intercept and slope of the linear regression lines (Table 4). The P values were obtained using Wald's test (significance codes: *** $P < 0.001$; ** $P < 0.01$; * $P < 0.05$).

onset STGD1 and AMD. We use an exploratory approach with different novel analysis strategies for detection of AFS that may reflect rarefaction of choroidal vasculature. Specifically, the approach included removal of decorrelation tail artifacts and optimization of the signal-to-noise ratio by downsizing of the images as well as compensation for signal attenuation by consideration of structural data. Additionally, a further conservative approach by exclusion of all areas of flecks and drusen was used to exclude “shadow artifacts” as potential confounder (Supplementary Material). Despite mimicking phenotypic manifestations of late-onset RPE atrophy, distinct differences

TABLE 4. Results of the Mixed-Effects Model (Estimate of Effect) for the Flow Texture Analysis

Variable	Estimate	SE*	P Value
γ -intercept (b)			
Age, $\log_{10}(n)/y$	-0.006	0.004	0.144
Area1, $\log_{10}(n)/mm^2$	0.073	0.010	<0.001
Diagnosis			
STGD1 vs. AMD, $\log_{10}(n)$	0.390	0.149	0.024
Control vs. AMD, $\log_{10}(n)$	0.609	0.143	<0.001
Slope (m)			
Age, $\log_{10}(n)/\log_{10}(\mu m^2)/y$	0.003	0.002	0.125
Area1, $\log_{10}(n)/\log_{10}(\mu m^2)/mm^2$	-0.018	0.004	<0.001
Diagnosis			
STGD1 vs. AMD, $\log_{10}(n)/\log_{10}(\mu m^2)$	-0.124	0.055	0.026
Control vs. AMD, $\log_{10}(n)/\log_{10}(\mu m^2)$	-0.202	0.053	<0.001

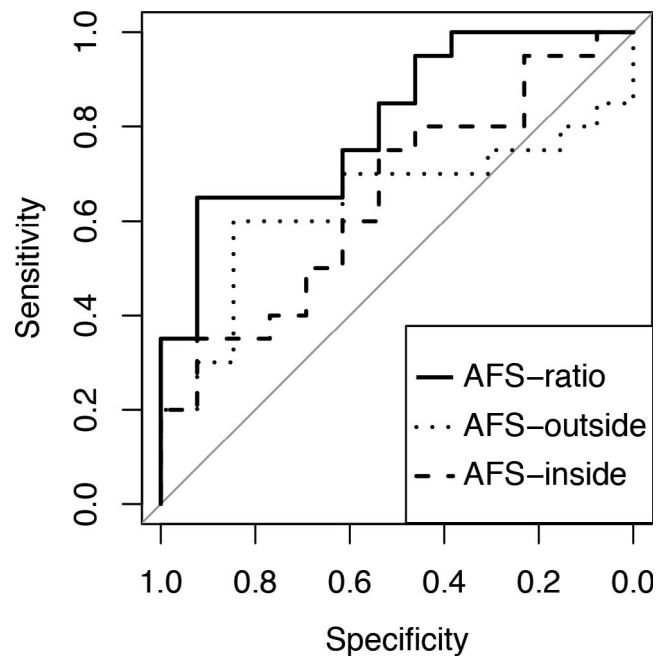
* Standard error.

between the two disease entities indeed were found regarding the AFS that may reflect rarefaction of choroidal vasculature. These differences were most pronounced outside of the RPE atrophy. Here, “absence-of-flow signals” was more pronounced in AMD, while inside RPE atrophy the absence of flow was more pronounced in STGD1.

Within areas of RPE atrophy, our findings are in line with recently published qualitative data that also found extensive alterations resulting in a loss of the CC flow signal texture indicating a putative loss of the CC and Sattler's layer in STGD1, whereas AMD patients showed only a rarefied CC flow signal texture.³⁰ These differences may also explain the hypofluorescence in areas of RPE atrophy during late phases of ICGA in STGD1, known as “dark atrophy.”²⁸ Previously, slower progression of RPE atrophy in STGD1 as compared to AMD was observed, implicating a relatively earlier onset of RPE atrophy in late-onset STGD1 as compared to AMD.⁵² Potentially, this difference in disease duration may explain to some extent the diverging degree of vascular density within RPE atrophy between these two disease entities.

Differences in the flow signal texture between the two diseases might also arise from differential pathomechanism. The preserved dense vascular network outside the RPE atrophy in STGD1 is compatible with the hypothesis of a primary outer retinal pathology followed by secondary atrophy of the choroid. Accordingly, choroidal thinning was shown to be absent in STGD1 eyes with mild phenotypes, but occurs in eyes with widespread disease manifestations and respective RPE atrophy, suggesting a diffusible factor from the RPE sustaining the choroidal structure as well as highlighting the importance of the complex interplays of outer retina, RPE, and choroid.^{18,53,54} Histopathologic studies of STGD1 are sparse and are missing for late-onset disease manifestation. Nevertheless, all reports so far describe a loss of CC within areas of RPE atrophy and preserved CC outside of RPE atrophy, compatible with our findings as we found no differences between STGD1 and controls outside of RPE atrophy.^{21–23} In contrast, AMD revealed reduced CC flow signal outside of RPE atrophy in this in vivo study as previously described by histologic data, suggesting that CC breakdown might precede outer retinal degeneration in AMD.²⁵ However, histologic studies concerning the CC outside of RPE atrophy in AMD report inconsistent results, which may be a result of AMD being a complex disease caused by differing underlying pathomechanisms.^{9,24,25}

Regarding biomarkers to predict disease progression, OCT-A alterations might not be suitable for STGD1, since no statistically significant differences for AFS area fraction outside of RPE atrophy between STGD1 and controls were found. With

**FIGURE 5.** Receiver operating characteristic (ROC) curves. The ROC curves for the diagnosis of STGD1 versus AMD based on the absence of flow (AFS) within atrophy of the retinal pigment epithelium (*dotted line*), outside of atrophy of the retinal pigment epithelium (*dashed line*), and the AFS ratio (*solid line*) reveal that the AFS ratio exhibits the highest diagnostic accuracy.

current understanding of the pathomechanism,^{4,5,55} measurement of lipofuscin accumulation might be more useful. As elevated FAF intensity is the first measurable change in STGD1,⁵⁵ the innovative in vivo imaging modality of quantitative FAF appears to be more suitable in this particular context.^{56–59} In AMD, the distinct alterations of the CC flow signal texture outside of atrophy might potentially be indicative of choroidal alterations beyond the area of complete RPE atrophy. A longitudinal comparison of these OCT-A alterations with the established FAF characteristics as prognostic determinants seems warranted.^{60–62}

Most recent advances in research led to currently ongoing and forthcoming trials probing new therapeutic strategies for STGD1 including visual cycle inhibitors, deuterated vitamin A, and gene therapy,^{12–15} as well as complement inhibition and neuroprotection for late-stage dry AMD (Ghosh C, et al. *IOVS* 2017;58:ARVO E-Abstract 1960).¹⁶ In order to avoid incorrect inclusion of patients leading to potential misinterpretation, differentiation of mimicking phenotyping features in STGD1 and AMD is crucial.¹¹ Multimodal imaging is an essential tool for assessing patients with retinal degenerations.⁶³ Regarding FAF, STGD1 may often be easily identified based on characteristic phenotypic features such as flecks, peripapillary sparing, and elevated FAF intensity.^{55–59,61,64} In contrast, AMD reveals different FAF patterns and low to low-normal FAF intensity.^{61,65} While good diagnostic separability is given for STGD1 and AMD based on FAF imaging and genetic testing, the study presented here outlines a framework that may now be used for subphenotype analysis within disease entities. For example, choroidal insufficiency has been previously implicated in the pathogenesis of subphenotypes within the spectrum of AMD including “reticular macular disease” and “diffuse-trickling geographic atrophy” based on indocyanine green and fluorescein angiography findings, pronounced choroidal thinning, and cardiovascular comorbidity.^{33–37}

Limitations of this study need to be considered. While STGD1 and AMD patients exhibited phenotypic differences inside of RPE atrophy, these differences appeared to be not adequately quantified by the AFS area fraction. As mentioned previously, larger choroidal vessels (putative venous vasculature from Haller's layer) shift to more superficial layers in RPE atrophy secondary to STGD1.¹⁸ Thus, large-caliber Haller's layer vessels were observed in the CC-slab (Fig. 2) of STGD1 and therefore counted as flow signal resulting in an overestimation of the flow signal in STGD1. Further, hyperreflective material within RPE atrophy, that potentially shadows the signal, was more common in AMD than STGD1. Therefore, the higher flow signal within RPE atrophy in AMD as compared to STGD1 most likely represents a conservative estimate. Concerning the AFS spots outside of RPE atrophy, concerns might arise that shadow artifacts may as well confound the results. The OCT device used in this study deploys a long-wavelength swept source (~1050 nm) providing presumably enhanced detection of signals from the deeper layers.⁶⁶ Therefore, deeper choroidal vessels were frequently visible in regions with CC flow signal loss (Figs. 2, 3), suggesting that at least in this subset of AFS spots, sufficient signal was available for detection of "true" CC dropout. Indeed, a recent study demonstrated that significantly fewer drusen are associated with reduced or absent flow signal in swept-source OCT compared to spectral-domain OCT.⁶⁷ Furthermore, the conservative approach via exclusion of all regions with a given RPE-drusen complex thickening from the analysis (cf. Ref. 47) yielded similar results. This indicates that it is rather unlikely that the results are secondary to shadow artifacts or RPE reflectivity. Nevertheless, the primary conservative analysis could bias the results, since reduced vascular density was shown colocalize to drusen in histologic studies. Accordingly, exclusion of these areas would lead to an overestimation of the vascular density.⁶⁸

In conclusion, using the present exploratory approach, this study provides evidence that phenotypic features on OCT-A imaging allow for differentiation between RPE atrophy secondary to STGD1 versus AMD that could support the selection of patients for emerging interventional trials.¹²⁻¹⁶ Further, these results suggest a differential role of the choroid in the pathogenesis of RPE atrophy secondary to STGD1 and geographic atrophy secondary to AMD that could interfere with treatment strategies. Especially in STGD1, severe degeneration of the CC within RPE atrophy could interfere with therapies aiming for replacement of photoreceptor and RPE cells.¹⁵ In AMD, the results shown here, albeit only cross-sectional, are compatible with vascular changes preceding RPE atrophy. Consequently, longitudinal studies in AMD investigating the precise temporal relationship between flow signal alterations in OCT-A, deposit formation in SD-OCT, and RPE atrophy in FAF seem warranted.

Acknowledgments

The authors thank Carl Zeiss Meditec, Inc., for the technical support and input, in particular from Stephanie Magazzeni and Mary Durbin.

Supported by the BONFOR GEROK Program of the Faculty of Medicine, University of Bonn, Grant O-137.0023 (PLM), Grant O-137.0022 (MP), Grant O-137.0025 (MP), and the German Research Foundation Grants MU4279/1-1 (PLM), LI2846/1-1 (ML), Ho1926/3-1 (FGH), FL658/4-1 (MF), and FL 658/4-2 (MF). The authors alone are responsible for the writing and content of the paper.

Disclosure: **P.L. Müller**, Heidelberg Engineering (F), Optos (F), Carl Zeiss Meditec (F), CenterVue (F); **M. Pfau**, Heidelberg Engineering (F), Optos (F), Carl Zeiss Meditec (F), CenterVue (F); **P.T. Möller**, Heidelberg Engineering (F), Optos (F), Carl Zeiss

Meditec (F), CenterVue (F); **J. Nadal**, None; **M. Schmid**, None; **M. Lindner**, Heidelberg Engineering (F), Optos (F), Carl Zeiss Meditec (F), CenterVue (F), Allergan (R); **L. de Sisternes**, Carl Zeiss Meditec (E); **H. Stöhr**, None; **B.H.F. Weber**, None; **C. Neuhaus**, None; **P. Herrmann**, Heidelberg Engineering (F), Optos (F), Carl Zeiss Meditec (F), CenterVue (F); **S. Schmitz-Valckenberg**, Heidelberg Engineering (F, R), Optos (F), Carl Zeiss Meditec (F), CenterVue (F), Allergan (F, R), Alcon/Novartis (F, R), Bioeq/Fermycon (F), Genentech/Roche (F, R), Bayer (F, R); **F.G. Holz**, Heidelberg Engineering (F, C, R), Optos (F), Carl Zeiss Meditec (F, C), CenterVue (F), Allergan (F, R), Alcon/Novartis (F, R), Genentech/Roche (F, R), Bayer (F, R), Acucela (F, R), Boehringer Ingelheim (F, R); **M. Fleckenstein**, Heidelberg Engineering (F, R), Optos (F), Carl Zeiss Meditec (F), CenterVue (F), Alcon/Novartis (F, R), Bayer (F, R), Alimera (F, R), P

References

- Hamel CP. Cone rod dystrophies. *Orphanet J Rare Dis.* 2007; 2:7.
- Kitiratschky VBD, Grau T, Bernd A, et al. ABCA4 gene analysis in patients with autosomal recessive cone and cone rod dystrophies. *Eur J Hum Genet.* 2008;16:812-819.
- Riveiro-Alvarez R, Lopez-Martinez M-A, Zernant J, et al. Outcome of ABCA4 disease-associated alleles in autosomal recessive retinal dystrophies: retrospective analysis in 420 Spanish families. *Ophthalmology.* 2013;120:2332-2337.
- Allikmets R, Singh N, Sun H, et al. A photoreceptor cell-specific ATP-binding transporter gene (ABCR) is mutated in recessive Stargardt macular dystrophy. *Nat Genet.* 1997;15: 236-246.
- Koenekoop RK. The gene for Stargardt disease, ABCA4, is a major retinal gene: a mini-review. *Ophthalmic Genet.* 2003; 24:75-80.
- Lois N, Holder GE, Bunce C, Fitzke FW, Bird AC. Phenotypic subtypes of Stargardt macular dystrophy-fundus flavimaculatus. *Arch Ophthalmol.* 2001;119:359-369.
- Fujinami K, Lois N, Mukherjee R, et al. A longitudinal study of Stargardt disease: quantitative assessment of fundus autofluorescence, progression, and genotype correlations. *Invest Ophthalmol Vis Sci.* 2013;54:8181-8190.
- Hoyng CB, Lambertus S, Bax NM. Stargardt disease. In: Querques G, Souied EH, eds. *Macular Dystrophies*. New York: Springer; 2016:25-30.
- Lim LS, Mitchell P, Seddon JM, Holz FG, Wong TY. Age-related macular degeneration. *Lancet.* 2012;379:1728-1738.
- Schmitz-Valckenberg S. The journey of "geographic atrophy" through past, present, and future. *Ophthalmologica.* 2017; 237:11-20.
- Saksens NTM, Fleckenstein M, Schmitz-Valckenberg S, et al. Macular dystrophies mimicking age-related macular degeneration. *Prog Retin Eye Res.* 2014;39:23-57.
- Charbel Issa P, Barnard AR, Herrmann P, Washington I, MacLaren RE. Rescue of the Stargardt phenotype in Abca4 knockout mice through inhibition of vitamin A dimerization. *Proc Natl Acad Sci U S A.* 2015;112:8415-8420.
- Schwartz SD, Hubschman J-P, Heilwell G, et al. Embryonic stem cell trials for macular degeneration: a preliminary report. *Lancet.* 2012;379:713-720.
- Han Z, Conley SM, Naash MI. Gene therapy for Stargardt disease associated with ABCA4 gene. *Adv Exp Med Biol.* 2014;801:719-724.
- Scholl HPN, Strauss RW, Singh MS, et al. Emerging therapies for inherited retinal degeneration. *Sci Transl Med.* 2016;8: 368rv6.
- Yaspan BL, Williams DE, Holz FG, et al. Targeting factor D of the alternative complement pathway reduces geographic

- atrophy progression secondary to age-related macular degeneration. *Sci Transl Med*. 2017;9:eaf1443.
17. Strauss O. The retinal pigment epithelium in visual function. *Physiol Rev*. 2005;85:845–881.
 18. Müller PL, Fimmers R, Gliem M, Holz FG, Charbel Issa P. Choroidal alterations in ABCA4-related retinopathy. *Retina*. 2017;37:359–367.
 19. Saint-Geniez M, Kurihara T, Sekiyama E, Maldonado AE, D'Amore PA. An essential role for RPE-derived soluble VEGF in the maintenance of the choriocapillaris. *Proc Natl Acad Sci U S A*. 2009;106:18751–18756.
 20. Kurihara T, Westenskow PD, Bravo S, Aguilar E, Friedlander M. Targeted deletion of Vegfa in adult mice induces vision loss. *J Clin Invest*. 2012;122:4213–4217.
 21. Birnbaach CD, Järveläinen M, Possin DE, Milam AH. Histopathology and immunocytochemistry of the neurosensory retina in fundus flavimaculatus. *Ophthalmology*. 1994;101:1211–1219.
 22. Eagle RC, Lucier AC, Bernardino VB, Yanoff M. Retinal pigment epithelial abnormalities in fundus flavimaculatus: a light and electron microscopic study. *Ophthalmology*. 1980;87:1189–1200.
 23. Klien BA, Krill AE. Fundus flavimaculatus. Clinical, functional and histopathologic observations. *Am J Ophthalmol*. 1967;64:3–23.
 24. McLeod DS, Grebe R, Bhutto I, Merges C, Baba T, Luty GA. Relationship between RPE and choriocapillaris in age-related macular degeneration. *Invest Ophthalmol Vis Sci*. 2009;50:4982–4991.
 25. Biesemeier A, Taubitz T, Julien S, Yoeruek E, Schraermeyer U. Choriocapillaris breakdown precedes retinal degeneration in age-related macular degeneration. *Neurobiol Aging*. 2014;35:2562–2573.
 26. Schwoerer J, Secrétan M, Zografos L, Piguet B. Indocyanine green angiography in fundus flavimaculatus. *Ophthalmologica*. 2000;214:240–245.
 27. Holz FG, Bellmann C, Rohrschneider K, Burk RO, Völcker HE. Simultaneous confocal scanning laser fluorescein and indocyanine green angiography. *Am J Ophthalmol*. 1998;125:227–236.
 28. Giani A, Pellegrini M, Carini E, Deiro AP, Bottoni F, Staurenghi G. The dark atrophy with indocyanine green angiography in Stargardt disease. *Invest Ophthalmol Vis Sci*. 2012;53:3999–4004.
 29. Fang PP, Harmening WM, Müller PL, Lindner M, Krohne TU, Holz FG. Technische Grundlagen der OCT-Angiographie [in German]. *Ophthalmologie*. 2016;113:6–13.
 30. Pellegrini M, Acquistapace A, Oldani M, et al. Dark atrophy: an optical coherence tomography angiography study. *Ophthalmology*. 2016;123:1879–1886.
 31. Strauss RW, Muñoz B, Ho A, et al. Incidence of atrophic lesions in Stargardt disease in the progression of atrophy secondary to Stargardt disease (ProgStar) study. *JAMA Ophthalmol*. 2017;53:841–852.
 32. Strauss RW, Muñoz B, Wolfson Y, et al. Assessment of estimated retinal atrophy progression in Stargardt macular dystrophy using spectral-domain optical coherence tomography. *Br J Ophthalmol*. 2016;100:956–962.
 33. Smith RT, Sohrab MA, Busuioc M, Barile G. Reticular macular disease. *Am J Ophthalmol*. 2009;148:733–743.e2.
 34. Schmitz-Valckenberg S, Steinberg JS, Fleckenstein M, Visvalingam S, Brinkmann CK, Holz FG. Combined confocal scanning laser ophthalmoscopy and spectral-domain optical coherence tomography imaging of reticular drusen associated with age-related macular degeneration. *Ophthalmology*. 2010;117:1169–1176.
 35. Fleckenstein M, Schmitz-Valckenberg S, Martens C, et al. Fundus autofluorescence and spectral-domain optical coherence tomography characteristics in a rapidly progressing form of geographic atrophy. *Invest Ophthalmol Vis Sci*. 2011;52:3761–3766.
 36. Fleckenstein M, Schmitz-Valckenberg S, Lindner M, et al. The “diffuse-trickling” fundus autofluorescence phenotype in geographic atrophy. *Invest Ophthalmol Vis Sci*. 2014;55:2911–2920.
 37. Fleckenstein M, Grassmann F, Lindner M, et al. Distinct genetic risk profile of the rapidly progressing diffuse-trickling subtype of geographic atrophy in age-related macular degeneration (AMD). *Invest Ophthalmol Vis Sci*. 2016;57:2463–2471.
 38. Boon CJF, van Schooneveld MJ, den Hollander AI, et al. Mutations in the peripherin/RDS gene are an important cause of multifocal pattern dystrophy simulating STGD1/fundus flavimaculatus. *Br J Ophthalmol*. 2007;91:1504–1511.
 39. Lambertus S, Lindner M, Bax NM, et al. Progression of late-onset Stargardt disease. *Invest Ophthalmol Vis Sci*. 2016;57:5186–5191.
 40. Early Treatment Diabetic Retinopathy Study Research Group. Early Treatment Diabetic Retinopathy Study design and baseline patient characteristics. ETDRS report number 7. *Ophthalmology*. 1991;98(5 suppl):741–756.
 41. Schmitz-Valckenberg S, Brinkmann CK, Alten F, et al. Semi-automated image processing method for identification and quantification of geographic atrophy in age-related macular degeneration. *Invest Ophthalmol Vis Sci*. 2011;52:7640–7646.
 42. Kuehlewein L, Hariri AH, Ho A, et al. Comparison of manual and semiautomated fundus autofluorescence analysis of macular atrophy in Stargardt disease phenotype. *Retina*. 2016;36:1216–1221.
 43. Pfau M, Goerdt L, Schmitz-Valckenberg S, et al. Green-light autofluorescence versus combined blue-light autofluorescence and near-infrared reflectance imaging in geographic atrophy secondary to age-related macular degeneration. *Invest Ophthalmol Vis Sci*. 2017;58:121–130.
 44. Zhang Q, Zheng F, Motulsky EH, et al. A novel strategy for quantifying choriocapillaris flow voids using swept-source OCT angiography. *Invest Ophthalmol Vis Sci*. 2018;59:203–211.
 45. Borrelli E, Uji A, Sarraf D, Sadda SR. Alterations in the choriocapillaris in intermediate age-related macular degeneration. *Invest Ophthalmol Vis Sci*. 2017;58:4792–4798.
 46. Phansalkar N, More S, Sabale A, Joshi M. Adaptive local thresholding for detection of nuclei in diversity stained cytology images. In: *2011 International Conference on Communications and Signal Processing*. IEEE; 2011:218–220.
 47. Spaide RF. Choriocapillaris flow features follow a power law distribution: implications for characterization and mechanisms of disease progression. *Am J Ophthalmol*. 2016;170:58–67.
 48. R Development Core Team. R: a language and environment for statistical computing. Vienna, Austria: R Foundation for Statistical Computing; 2013.
 49. Pinheiro J, Bates D, DebRoy S, Sarkar D; R Core Team. NLME: linear and nonlinear mixed effects models (R package version 3.1-117, 2014). Available at: <https://CRAN.R-project.org/package=nlme>. Accessed July 25, 2018.
 50. Schulz HL, Grassmann F, Kellner U, et al. Mutation spectrum of the ABCA4 gene in 335 Stargardt disease patients from a multicenter German cohort—impact of selected deep intronic variants and common SNPs. *Invest Ophthalmol Vis Sci*. 2017;58:394–403.

51. Zernant J, Lee W, Collison FT, et al. Frequent hypomorphic alleles account for a significant fraction of ABCA4 disease and distinguish it from age-related macular degeneration. *J Med Genet.* 2017;54:404–412.
52. Lindner M, Lambertus S, Mauschitz MM, et al. Differential disease progression in atrophic age-related macular degeneration and late-onset Stargardt disease. *Invest Ophthalmol Vis Sci.* 2017;58:1001–1007.
53. Yeoh J, Rahman W, Chen F, et al. Choroidal imaging in inherited retinal disease using the technique of enhanced depth imaging optical coherence tomography. *Graefes Arch Clin Exp Ophthalmol.* 2010;248:1719–1728.
54. Bertelsen M, Zernant J, Larsen M, Duno M, Allikmets R, Rosenberg T. Generalized choriocapillaris dystrophy, a distinct phenotype in the spectrum of ABCA4-associated retinopathies. *Invest Ophthalmol Vis Sci.* 2014;55:2766–2776.
55. Cideciyan AV, Aleman TS, Swider M, et al. Mutations in ABCA4 result in accumulation of lipofuscin before slowing of the retinoid cycle: a reappraisal of the human disease sequence. *Hum Mol Genet.* 2004;13:525–534.
56. Delori FC, Staurenghi G, Arend O, Dorey CK, Goger DG, Weiter JJ. In vivo measurement of lipofuscin in Stargardt's disease-fundus flavimaculatus. *Invest Ophthalmol Vis Sci.* 1995;36:2327–2331.
57. Delori F, Greenberg JP, Woods RL, et al. Quantitative measurements of autofluorescence with the scanning laser ophthalmoscope. *Invest Ophthalmol Vis Sci.* 2011;52:9379–9390.
58. Burke TR, Duncker T, Woods RL, et al. Quantitative fundus autofluorescence in recessive Stargardt disease. *Invest Ophthalmol Vis Sci.* 2014;55:2841–2852.
59. Müller PL, Gliem M, Mangold E, et al. Monoallelic ABCA4 mutations appear insufficient to cause retinopathy: a quantitative autofluorescence study. *Invest Ophthalmol Vis Sci.* 2015;56:8179–8186.
60. Schmitz-Valckenberg S, Bindewald-Wittich A, Dolar-Szczasny J, et al. Correlation between the area of increased autofluorescence surrounding geographic atrophy and disease progression in patients with AMD. *Invest Ophthalmol Vis Sci.* 2006;47:2648–2654.
61. Holz FG, Bindewald-Wittich A, Fleckenstein M, Dreyhaupt J, Scholl HPN, Schmitz-Valckenberg S. Progression of geographic atrophy and impact of fundus autofluorescence patterns in age-related macular degeneration. *Am J Ophthalmol.* 2007;143:463–472.
62. Niu S, de Sistiernes L, Chen Q, Rubin DL, Leng T. Fully automated prediction of geographic atrophy growth using quantitative spectral-domain optical coherence tomography biomarkers. *Ophthalmology.* 2016;123:1737–1750.
63. Holz FG, Sadda SR, Staurenghi G, et al. Imaging protocols in clinical studies in advanced age-related macular degeneration: recommendations from Classification of Atrophy Consensus Meetings. *Ophthalmology.* 2017;124:464–478.
64. Boon CJF, Jeroen Klevering B, Keunen JEE, Hoyng CB, Theelen T. Fundus autofluorescence imaging of retinal dystrophies. *Vision Res.* 2008;48:2569–2577.
65. Gliem M, Müller PL, Finger RP, McGuinness MB, Holz FG, Charbel Issa P. Quantitative fundus autofluorescence in early and intermediate age-related macular degeneration. *JAMA Ophthalmol.* 2016;134:817–824.
66. Miller AR, Roisman L, Zhang Q, et al. Comparison between spectral-domain and swept-source optical coherence tomography angiographic imaging of choroidal neovascularization. *Invest Ophthalmol Vis Sci.* 2017;58:1499–1505.
67. Lane M, Moulton EM, Novais EA, et al. Visualizing the choriocapillaris under drusen: comparing 1050-nm swept-source versus 840-nm spectral-domain optical coherence tomography angiography. *Invest Ophthalmol Vis Sci.* 2016;57:OCT585–OCT590.
68. Mullins RF, Johnson MN, Faidley EA, Skeie JM, Huang J. Choriocapillaris vascular dropout related to density of drusen in human eyes with early age-related macular degeneration. *Invest Ophthalmol Vis Sci.* 2011;52:1606–1612.